y direction will be

$$H_{yp}(t)=GSe_{yz}(t)/\gamma_e\hbar. \quad \text{(B1)}$$

This perpendicular field will oscillate at the frequency of the strain and will act on the magnetization as an additional anisotropy field. At a given instant of time the magnetization will precess about the new anisotropy direction, and the precessional axis will oscillate about the z axis with the frequency of the impressed strain as indicated in Fig. 1(b). The assumption, of course, has been made that the precessional frequency is much greater than the phonon frequency. Let us now turn our consideration to the nucleus. We see from the isotropic form of the hyperfine interaction (2.4), that the nucleus will experience a magnetic field due to the electrons of

$$\mathbf{H}_n(t)=A\langle\mathbf{S}(t)\rangle/\gamma_n\hbar. \quad \text{(B2)}$$

The perpendicular field component at the nucleus is then

$$H_{yn}(t)=AS\sin\theta(t)/\gamma_n\hbar\cong AS^2Ge_{yz}(t)/\gamma_n\gamma_e\hbar^2H_A. \quad \text{(B3)}$$

Here we have taken $\sin\theta(t)\cong\theta(t)=H_{yp}(t)/H_A$. Considering the same for the x direction, we obtain the net coupling of the strain to the jth nucleus;

$$V_{npj}(t)=\hbar\gamma_n\mathbf{H}_{\perp j}(t)\cdot\mathbf{I}_j$$
$$=(AS^2G/2\hbar\omega_A)[I_j^+e_{-zj}(t)+I_j^-e_{+zj}(t)], \quad \text{(B4)}$$

which is exactly the form as derived from spin-wave theory.

PHYSICAL REVIEW VOLUME 132, NUMBER 3 1 NOVEMBER 1963

Magnetic Resonance Studies of Unpaired Atoms in Solid D_2*

MARK SHARNOFF† AND R. V. POUND
Lyman Laboratory, Harvard University, Cambridge, Massachusetts
(Received 27 June 1963)

We have studied the ground-state spectroscopic parameters, line shapes and breadths, relaxation times, and saturation behavior of unpaired atoms produced in samples of solid D_2 containing up to 1 at.% T_2. The D-atom electron spin resonance spectrum was found at 24 000 Mc/sec to consist of three composite lines in which the peaks of a broad component and a narrow component coincided. This result is interpreted by assuming that there are two different types of lattice sites for the unpaired atoms. The site responsible for the narrow line is tentatively identified, on the basis of linebreadth, as an interstitial located at the center of the square face of a unit cell having a D_2 molecule at each vertex. The other site has not been identified. The narrowline sites appear to become populated about 10 times more rapidly than the broadline sites. Linebreadths ranged from 2.2 G at 4.2°K to 44.5 G at 1.17°K. The effective spectroscopic splitting factor and hyperfine-structure interactions of the D, T, and H atoms were found to differ by only fractions of a percent from their free atomic values. The relaxation times of the D-atom spectra show little sensitivity to lattice temperature over the range from 1.2° to 4.2°. The relaxation time of the interstitial spins varies from 2 sec to 220 msec depending upon the concentration of atoms in the lattice. The relaxation time of spins in the broadline sites is in the neighborhood of 220 msec. From the presence of strong diagonal relaxation it is argued that the mechanism which relaxes the broadline D atoms has a correlation time of about 10^{-8} sec. The behavior of the interstitial spin relaxation is interpreted in terms of a model in which spin polarization from these atoms diffuses by the Bloembergen mechanism to the broadline sites, where relaxation takes place. The model clarifies quantitatively the differences between the relaxation behavior of D atoms on the one hand and the far less numerous T and H atoms on the other. The resonance lines are homogeneously broadened as a rule. Inconsistencies between the results of saturation studies and the measured relaxation times are shown to be due to an anomalous line narrowing and intensification after the onset of saturation. The anomaly appears to be characteristic only of the narrow line component.

INTRODUCTION

SEVERAL years ago we undertook a series of investigations intended to demonstrate the feasibility of producing an isotopically pure target of polarized deuterium nuclei for use with medium and high-energy particle accelerators. The advantages of a polarized D_2 target are apparent; it serves as a source of both polarized protons and polarized neutrons, and it is without the background scattering from heavy, unpolarized nuclei produced from polarized targets of polyethylene or of the complex rare earth salt, $(La,Nd)_2Mg_3(NO_3)_{12}\cdot 24H_2O$, with which the Berkeley group has had such success.[1] With these attractive features in mind, we sought to develop techniques for producing unpaired electron spins within a solid D_2 matrix, whose polariza-

* Work supported in part by the U. S. Atomic Energy Commission and the U. S. Office of Naval Research. Part of this work is taken by a thesis submitted by Mark Sharnoff to the Faculty of Arts and Sciences, Harvard University, in partial fulfillment of the requirements for the degree of Doctor of Philosophy, 1963.

† National Science Foundation Predoctoral Fellow, 1959–61. Present address: National Bureau of Standards, Washington 25, D. C.

[1] T. J. Schmugge and C. D. Jeffries, Phys. Rev. Letters 9, 268 (1962).

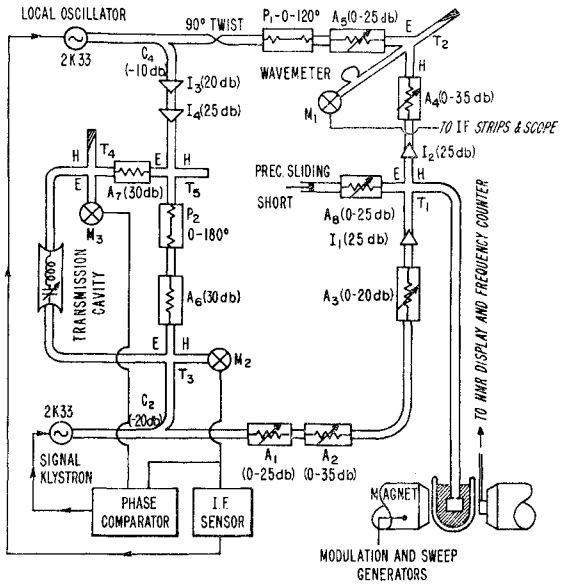

FIG. 1. Schematic diagram of the magnetic resonance spectrometer.

tion could be transferred dynamically to the system of D_2 nuclei by familiar methods[2] employing forbidden paramagnetic transitions.

In our early experiments we employed a technique similar to that used by Jen *et al.*,[3] in which the products of a discharge in gaseous deuterium were condensed upon a surface which was in good thermal contact with a bath of liquid helium. This work indicated that solid D_2 containing unpaired D atoms had promise[4] as a working substance for the dynamic polarization scheme, the limitations[5] observed in the enhancements of our D_2 nuclear magnetic resonance signals proceeding apparently from limitations in the concentrations of D atoms obtainable when reasonable discharge condensation rates were employed.

In order to overcome this technical limitation, we prepared several samples by freezing a mixture of 99 parts deuterium and 1 part tritium. The saturation concentration of unpaired atoms in such samples should reflect chemical kinetics which are intrinsic to the cold lattice rather than the overheating of the condensing substrate characteristic of the experiments employing the discharge. The average concentration of unpaired atoms in our tritiated samples in fact exceeded by an order of magnitude or more those obtained in typical discharge samples of comparable size; but, to our surprise, our dynamic nuclear polarization attempts worked less effectively in the tritiated samples than in the discharge condensates.

In order to clarify the discrepancy in the behavior of the two types of samples, we carried out a rather extensive set of electron paramagnetic resonance studies of the atoms produced in the tritiated samples.

APPARATUS AND TECHNIQUE

The Microwave Spectrometer

Because the electron-spin-resonance (ESR) signals from our samples, all saturated at very low microwave power levels, it was found expedient to use a superheterodyne spectrometer to study them. Figure 1 illustrates this instrument, and Fig. 2 is a block diagram of the associated electronics, the circuits of which are largely of conventional design. The essential components of the spectrometer are the two 2K33 klystrons, which operate in the neighborhood of 23 940 Mc/sec; the microwave bridge T_1, one arm of which contains the resonant cavity housing the sample; and the mixer crystal M_1. The klystron frequencies are stabilized by the components in the branch intervening between directional couplers C_2 and C_4. The intermediate frequency is stabilized directly from mixer crystal M_2, while the phase difference between the coherent i.f. signals developed at M_2 and M_3 is used to derive a correction signal which stabilizes the frequency of the signal klystron with respect to the resonant frequency of the transmission cavity. Attenuators A_6 and A_7 were installed to ensure that there was effectively only one signal path connecting each klystron with either of the mixer crystals M_2 and M_3, thus preventing undesired interaction between the two AFC loops. The close similarity of the i.f. amplifiers, and the near equality in the electrical line lengths between the local oscillator and the two mixer crystals also reduced parasitic AFC loop interactions.

The arrangement of the remaining components of the spectrometer was suggested by our desire to make satu-

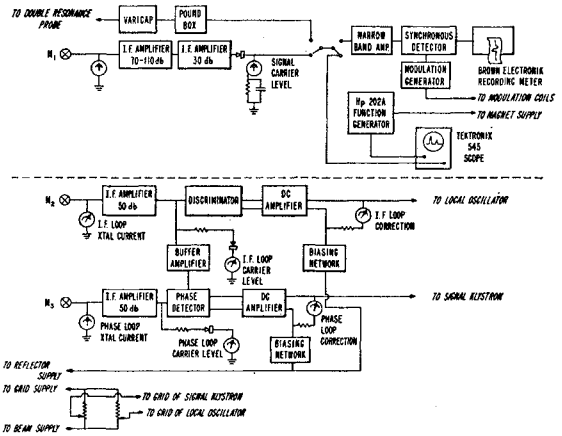

FIG. 2. Block diagram of the electronics of the spectrometer.

[2] O. S. Leifson and C. D. Jeffries, Phys. Rev. **122**, 1781 (1961).
[3] C. K. Jen, S. N. Foner, E. L. Cochran, and V. A. Bowers, Phys. Rev. **112**, 1169 (1958).
[4] G. A. Rebka, Jr., and M. Waine, Bull. Am. Phys. Soc. **7**, 538 (1962).
[5] Mark Sharnoff, Jack T. Sanderson, and R. V. Pound, Bull. Am. Phys. Soc. **7**, 538 (1962).

ration studies of the ESR signals. Attenuators A_2 and A_4 could be coordinated to vary the signal klystron power incident upon the sample cavity without changing that incident upon mixer crystal M_1. Saturation measurements were thus free from the variations in the mixer conversion efficiency which accompany large variations in the amplitude of the low-level carrier. Our saturation studies routinely involved variations of as much as 40 dB in the microwave power incident upon the cavity, which could be handled effectively by means of the coordinated attenuators. With the i.f. strip gains set at their usual levels, the conversion efficiency of M_1 and the over all gain of the i.f. strips proved constant over nearly the entire scale of the 100-μA meter at the second detector. The detection system was thus linear over a dynamic range sufficient to handle all the signals we encountered in our experiments. The time constant at the output of the second detector was 5×10^{-4} sec.

A second requirement for reliable saturation measurements is that the impedance of the microwave bridge, when set to suppress dispersion, should be invariant respecting changes in the settings of neighboring attenuators. This requirement was met by straddling the microwave bridge with isolators I_1 and I_2, which reduced by a factor of 300 or more the effect of standing waves between the bridge and neighboring components. The isolators between directional coupler C_4 and the tee T_5 were inserted in order to eliminate undesirable interference between the weak signal klystron carrier reaching M_1 via the microwave bridge T_1 and that reaching M_1 via the path through C_2, T_3, T_5, C_4, and A_5. The efficacy of these arrangements was demonstrated by the persistence of the symmetry of the absorption derivatives, even under extreme saturation.

Isolator I_2 performs the additional function of reducing the leakage of local oscillator power into the sample cavity. Attenuator A_5 was generally set so that the local oscillator produced 350μ A of dc current flowing in M_1.

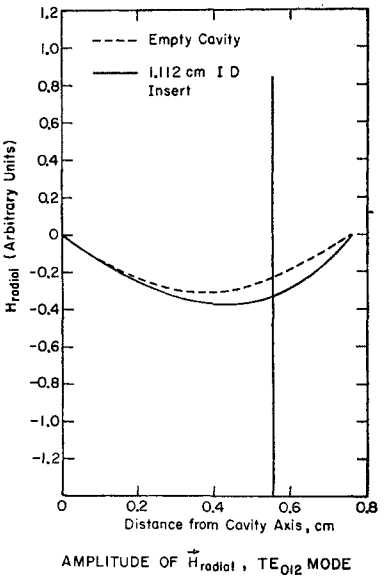

FIG. 4. Radial variation of H_{radial}. The curves end at the radius of the cavity, which is 0.770 cm.

The Sample Cavity

The cavity (Fig. 3) into which the tritiated samples were condensed was designed for the dynamic polarization studies and is therefore somewhat more complicated than desirable for simple ESR work. The cavity was operated in the circularly symmetric TE_{012} mode.[6] A nuclear magnetic resonance (NMR) pickup coil was mounted on a teflon coil form placed within the cavity. The entire system in which the tritium was contained was highly resistant to thermal and mechanical shock and reliably vacuum tight, even under repeated cyclings between room temperature and 1.2°K. Because of teflon's large coefficient of thermal expansion, the coil was machined 1% oversize in all dimensions and cooled in liquid nitrogen before being inserted into the cavity.

The configuration of the NMR coil was that of a rectangle whose short edges were bisected by the axis of the cavity. The wire thus lay in a plane perpendicular to the electric field of the TE_{01} modes, whose lines of force are circles about the cavity axis. The surface charge and current densities of the wire automatically support the continued existence of the TE_{01} modes, and the field configurations of these modes are identical, apart from higher nonpropagating modes which ensure that the electromagnetic fields will vanish inside the

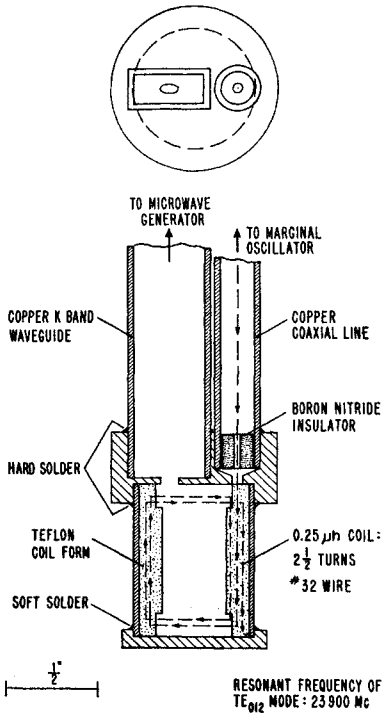

FIG. 3. The electron-nuclear double resonance cavity assembly.

[6] C. G. Montgomery, R. H. Dicke, and E. M. Purcell, *Principles of Microwave Circuits* (McGraw-Hill Book Company, Inc., New York, 1948).

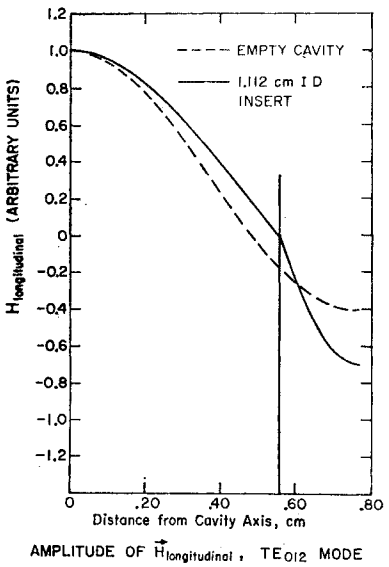

FIG. 5. Radial variation of $H_{\text{longitudinal}}$.

wire, from those which obtained before the wire was inserted. Since the coil is entirely coplanar with the magnetic field vectors of the TE_{01} modes, no microwave emf's will be induced around it, and no microwave energy will be coupled into the coaxial line. The external magnetic field, supplied by a Varian VA-1200 electromagnet, is perpendicular to the cavity axis and coplanar with the coil.

With a coil form having a low dielectric constant like teflon ($\epsilon=2.05$), the TE_{012} mode magnetic fields in the cavity-coil system are not very different from those pertaining to the empty cavity. Figures 4 and 5 compare the radial variation of the transverse and longitudinal components of the magnetic fields in a typical cross section with the Bessel functions J_1 and J_0 which characterize the resonance of the empty cavity. A visual comparison shows that the filling factor[7] of a sample in the form of a thin wafer occupying the entire bottom plate of the cavity will be approximately the same in the empty cavity as in the cavity containing the teflon insert and coil. The filling factor in the first of these instances may be evaluated from the normalization constants for the Bessel functions. Taking the dimensions of the cavity to be 0.606-in. diam by 0.915-in. long, and noting that only half the energy stored in the transverse magnetic field is associated with components perpendicular to the external magnetic field, we find for very thin samples a filling factor of

$$\eta=\frac{1}{2}\int_{\text{sample}} H_{\text{trans}}^2 dV \Big/ \int_{\text{cavity}} (H_{\text{trans}}^2+H_{\text{long}}^2)dV$$
$$=V_{\text{sample}}/V_{\text{cavity}}\left[1+\left(\frac{3.832}{\frac{4}{3}\pi}\right)^2\left(\frac{-J_0(3.832)}{J_2(3.832)}\right)\right]^{-1}. \quad (1)$$
$$=0.54(V_{\text{sample}}/V_{\text{cavity}}).$$

[7] G. Feher, Bell System Tech. J. 36, 449 (1957).

The oversize dimensions of the coil form (Fig. 3) are 0.612-in. o.d. by 0.438-in. i.d. by 0.925-in. long, the recesses in the ends being 0.130-in. deep by 0.518-in. diam. The TE_{012} mode resonance frequency of the completed cavity-coil assembly was 23 940 Mc/sec, and its Q exceeded 10 000 at 77°K. Higher values would doubtless have resulted had the cavity been made of electrolytically pure copper. When mounted within the closed cavity, the $2\frac{1}{2}$ turn coil customarily used had an inductance of about $\frac{1}{4}$ μH and a Q of 65 at 25 Mc/sec.

Sample Preparation

Samples were generally formed from a mixture of 400 cm³ (NTP) of deuterium gas with a desired amount, usually 4 cm³, of tritium gas. The sample reservoir was equipped with a pressure gauge, whose reading was useful in indicating the beginning of the condensation process. After being precooled in liquid nitrogen, the cavity-coil system was lowered gradually into the liquid helium chamber of the cryostat until the condensation began, whereupon it was held stationary for two or three minutes until the process had been completed. It is highly likely, because of the low thermal conductivity of teflon, the distribution of mass in the cavity assembly, and the method by which the sample was frozen, that the sample occupied a wafer-shaped region at the bottom of the cavity.

THEORETICAL CONSIDERATIONS

In the course of our experimentation we made accurate measurements of the effective hyperfine-coupling constants and spectroscopic splitting factors of the unpaired atoms produced in our samples, studied the shapes and breadths of the resonances and measured their absolute intensities, and made detailed saturation and relaxation investigations. In this section we present some elementary theory which will be useful in our discussion of these studies.

Spectroscopy

The spin Hamiltonian of a hydrogen-like atom, which has only one electron not in a closed shell, in a uniform magnetic field, $\mathbf{H}$, is[8]

$$\mathcal{H}=hA\mathbf{I}\cdot\mathbf{J}+(g_J\mu_0\mathbf{J}-g_I\mu_0\mathbf{I})\cdot\mathbf{H}, \quad (2)$$

where $\mathbf{I}$ and $\mathbf{J}$ are the total angular-momentum operators of the nucleus and the electron, respectively, and where the spectroscopic splitting factors g_I and g_J are related to the nuclear and electromagnetic moments $\boldsymbol{\mu}_I$ and $\boldsymbol{\mu}_J$ by

$$\boldsymbol{\mu}_I=g_I\mu_0\mathbf{I}; \quad \boldsymbol{\mu}_J=-g_J\mu_0\mathbf{J}. \quad (3)$$

The minus sign is included to make g intrinsically positive for the electron; μ_0 is the Bohr magneton,

[8] Norman F. Ramsey, *Molecular Beams* (Oxford University Press, New York, 1956).

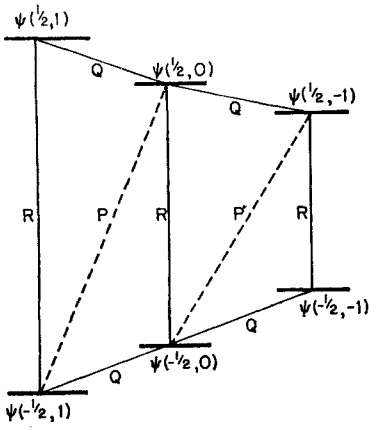

FIG. 6. Magnetic energy levels and transitions of a D atom in a high-external magnetic field.

0.92732×10^{-20} erg/G. The hyperfine coupling constant, hA, measures the strength of the interaction between the nuclear spin and the electronic angular momentum.

The approximate energy levels of an S-state deuterium atom in a high magnetic field, where the hyperfine interaction makes only a small contribution to the total magnetic energy, are illustrated in Fig. 6. The states have been labelled by their approximate electronic and nuclear spin projections, in units of $\hbar$, along the external magnetic field. Also illustrated in the diagram are some of the various transitions which can be induced by alternating magnetic fields of appropriate frequency. The transitions R, induced by alternating magnetic fields perpendicular to the uniform steady field, are allowed transitions and would occur even in the limit of vanishing hyperfine interaction. They correspond to a reorientation of the electronic spin and, hence, may be labelled by the projection I_z' of the nuclear spin, which is unchanged by the transition.

The remaining transitions are "first forbidden" and have intensities vastly lower than the R transitions. Those labeled Q have matrix elements reduced from those of the R transitions by the factor $Ah/2^{1/2}g_S\mu_0H_0$ and, hence, are induced, under the conditions of our experiments, some 24 000 times less readily than the R processes. The same is true of the P transitions, which are induced by alternating fields parallel to the external magnetic field. Other transitions, such as that connecting $\psi(-\frac{1}{2}, 1)$ and $\psi(\frac{1}{2}, -1)$, are more highly forbidden and will not be considered further.

Exact expressions for the energy levels of the spin Hamiltonian (2) are provided, when $J=\frac{1}{2}$ or $I=\frac{1}{2}$, by the Breit-Rabi formula,[9] which is most conveniently written in terms of the quantum numbers appropriate to the low-field limit:

$$E(F,m)=\frac{-\Delta W}{2(2I+1)}-\frac{\mu_I}{I}Hm\pm\frac{\Delta W}{2}\left[1+\frac{4mx}{2I+1}+x^2\right]^{1/2}. \quad (4)$$

Here ΔW is the hyperfine splitting between the two multiplets, $F=I+\frac{1}{2}$ and $F=I-\frac{1}{2}$, degenerate at $H=0$ ($\Delta W=Ah(I+\frac{1}{2})$), and x is given by

$$x=\frac{g_J-g_I}{\Delta W}\mu_0H. \quad (5)$$

The quantum numbers F and m are, respectively, the magnitude and the projection along $\mathbf{H}$, in units of $\hbar$, of the total angular momentum, $\mathbf{F}=\mathbf{J}+\mathbf{I}$, of the zero-field state which goes over into the state in question when the external field is applied. The plus sign in Eq. (4) is used when $F=I+\frac{1}{2}$ and the minus sign when $F=I-\frac{1}{2}$.

The allowed transitions I_z' of Fig. 6 correspond to the following transitions in (F,m) notation:

$$\begin{aligned}
&I_z'=I, && (I+\tfrac{1}{2}, I+\tfrac{1}{2})\leftrightarrow(I-\tfrac{1}{2}, I-\tfrac{1}{2});\\
&I_z'=I-1, && (I+\tfrac{1}{2}, I-\tfrac{1}{2})\leftrightarrow(I-\tfrac{1}{2}, I-\tfrac{3}{2});\\
&\cdots\\
&I_z'=-I, && (I+\tfrac{1}{2}, -I+\tfrac{1}{2})\leftrightarrow(I+\tfrac{1}{2}, -I-\tfrac{1}{2}).
\end{aligned}$$

The Bohr frequency conditions for the transitions $I_z'=\pm I$ will read

$$h\nu_I=\frac{\Delta W}{2}\left[1+x_I+\left\{1+2\frac{2I-1}{2I+1}x_I+x_I^2\right\}^{1/2}\right]-\frac{\mu_I}{I}H_I \quad (6)$$

$$h\nu_{-I}=\frac{\Delta W}{2}\left[-1+x_{-I}+\left\{1-2\frac{2I-1}{2I+1}x_{-I}+x_{-I}^2\right\}^{1/2}\right]-\frac{\mu_I}{I}H_{-I}; \quad (7)$$

and if I is integral, the transition $I_z'=0$ will satisfy

$$h\nu_0=\frac{\Delta W}{2}\left[\left\{1+2\frac{2I-1}{2I+1}x_0+x_0^2\right\}^{1/2}+\left\{1-2\frac{2I-1}{2I+1}x_0+x_0^2\right\}^{1/2}\right]-\frac{2I-1}{I}\mu_IH_0. \quad (8)$$

The subscripts of ν, x, and H refer to the I_z' designation.

The exact inversion of Eqs. (6) and (7) is a straightforward process which can be carried through regardless of the value of I. With the help of the abbreviations

$$e_+=h\nu_I+\frac{\mu_I}{I}H_I \quad (9)$$

and

$$e_-=h\nu_{-I}+\frac{\mu_I}{I}H_{-I} \quad (10)$$

and the definition

$$r=\frac{x_I}{x_{-I}}=\frac{H_I}{H_{-I}}, \quad (11)$$

[9] G. Breit and I. I. Rabi, Phys. Rev. 38, 2082 (1931).

the squares of Eqs. (6) and (7) become

$$\frac{1}{2I+1}x_I(\Delta W)^2-e_+x_I\Delta W-e_+\Delta W=-e_+^2, \quad (12)$$

$$\frac{1}{2I+1}x_I(\Delta W)^2+e_-x_I\Delta W-re_-\Delta W=re_-^2. \quad (13)$$

Subtraction of the second of these equations from the first gives

$$W=\frac{e_+^2+re_-^2}{(e_++e_-)x_I+(e_+-re_-)}. \quad (14)$$

When this equation is substituted into (12), an equation only quadratic in x_I is formed,

$$Ax_I^2+Bx_I+C=0, \quad (15)$$

with

$$A=e_+e_-(e_++e_-)(e_+-re_-), \quad (15a)$$

$$B=\frac{1}{2I+1}(e_+^2+re_-^2)^2-e_+(e_+^2+re_-^2)\times\{(e_++e_-)+(e_+-re_-)\}+2e_+^2(e_++e_-)(e_+-re_-), \quad (15b)$$

and

$$C=-e_+e_-(re_++e_-)(e_+-re_-). \quad (15c)$$

When the coefficients have been numerically evaluated, the quadratic formula may be used to find x_I, whereupon ΔW is immediately determined by (14). The value of g_J is subsequently found from (5). The nuclear spectroscopic splitting factor, g_I, may be taken for all but the most precise work from nuclear magnetic resonance measurements, the chemical shifts in these values being less than $10^{-4}\ g_I\sim10^{-7}\ g_J$.

When I is integral, an independent, highly accurate determination of g_J may be found by expanding (8). Terms in odd powers of x_0 will vanish, and the expression

$$g_J=\left(h\nu_0+\frac{2I-1}{I}\mu_IH_0\right)\times\left\{\mu_0H_0\left[1-\frac{4I^2-12I+1}{2(2I+1)^2}\frac{1}{x_0^2}\right]\right\}^{-1}, \quad (16)$$

will be accurate, for the conditions of the experiments below, where $x_0\gtrsim70$, to within one part in 10^8. The presence of electric quadrupole or higher order interactions between the atomic nucleus and its environment, which have been deleted from the spin-Hamiltonian (2), may be confirmed by using all possible combinations of the R transitions to determine g_J and A. If the various independent determinations agree within experimental error, the experiment has not been sufficiently precise to detect the presence of quadrupole effects.

Linebreadth

In this section we will concern ourselves with the line broadening to be expected from magnetic dipolar interactions of the form

$$\mathcal{H}_{12}=\frac{g_1g_2\mu_0^2}{r_{12}^3}\left[\mathbf{S}_1\cdot\mathbf{S}_2-\frac{3}{r_{12}^3}(\mathbf{S}_1\cdot\mathbf{r}_{12})(\mathbf{S}_2\cdot\mathbf{r}_{12})\right],$$

between a given unpaired atomic spin and the nuclear and atomic spins in the lattice in which it is embedded. The ESR lines we observed were symmetrical and in essence free of fine structure and may, for the present purposes, be described by their second and fourth moments about their centers. If $f(\omega)$ represents the line profile, normalized to unity on the frequency scale, the moments may be taken to be

$$M_{2n}=\int_{-\infty}^{\infty}(\omega-\omega_0)^{2n}f(\omega)d\omega, \qquad n=0,\ 1,\ 2,\ \cdots, \quad (17)$$
$$M_{2n+1}=0,$$

where ω_0 is the resonance frequency of the line in question. The normalization condition on f implies $M_0=1$. The higher moments are progressively more sensitive to the wings of the line profile, and consideration of only the second and fourth moments will give comparatively little information thereon.

Van Vleck[10] has provided a basis for calculation of the moments of all lines whose breadths arise from perturbations which are describable in a formalism not explicitly dependent upon time. Van Vleck's expression for the second moment of a resonance line whose breadth originates from magnetic dipolar interactions between the various spins in our samples is

$$M_2=\langle\Delta\omega^2\rangle_{\rm av}=\frac{1}{3}\left(\frac{g_Sg_I\mu_0^2}{\hbar}\right)^2I(I+1)\cdot(4/9)\sum_j b_{ij}^2+\frac{1}{3}\frac{g_S^4\mu_0^4}{\hbar^2}S(S+1)\left[\sum_k b_{ik}^2+(4/9)\sum_1 b_{i1}^2\right], \quad (18)$$

where

$$b_{im}=\frac{3}{2}\left(\frac{1-3\cos^2\theta_{im}}{r_{im}^3}\right), \quad (19)$$

and where g_I and g_S are the nuclear and electronic g factors and $\mathbf{r}_{ij}$ and $\mathbf{r}_{ik}$ are the radius vectors from the ith unpaired atom to the nuclear spins I_j and the remaining unpaired electronic spins S_k and S_1. The spins S_k are all in the same hyperfine state as S_i, the spins S_1 in remaining hyperfine states. We assume that the lattice is rigid, so that the vectors $\mathbf{r}_{im}$ are constants. The sums converge as r^{-4} and will be independent of the value of the index i.

The first lattice sum in Eq. (18), which expresses the contribution of nuclear magnetic moments to the linewidth, may be easily evaluated if the lattice is polycrystalline. (See Fig. 7.) For a polycrystalline body-centered tetragonal[11] lattice whose lattice vectors[11] bear

[10] J. H. Van Vleck, Phys. Rev. **74**, 1168 (1948).
[11] G. H. Wannier, *Elements of Solid State Theory* (Cambridge University Press, New York, 1959).

the ratio $c/a=1.73$,[12] this contribution is

$$M_{2,\mathrm{nuc}}=10.4g_I^2g_S^2\mu_0^4\frac{D(D+1)}{\hbar^2a^6}, \tag{20}$$

where D is the total nuclear spin of the deuterium molecule ($D=0$, 1, 2). It has been assumed that the unpaired atom is substitutional.

The evaluation of the second and third sums of Eq. (18), which contain the contribution of atomic spins to the linewidths, is less straightforward because the sums are carried only over the sites actually occupied by the atoms. If the lattice is randomly populated by these atoms, the evaluation of Kittel and Abrahams[13] may be used, and the partial sums easily related to sums taken over *all* the lattice sites. If only one atomic species, which has $2I+1$ hyperfine sublevels, is involved, and if p is the probability that any given lattice site is populated by an unpaired atom, then

$$\sum_k b_{ik}^2+(4/9)\sum_1 b_{i1}^2 =\frac{p}{2I+1}\sum_j b_{ij}^2+\frac{4}{9}\frac{2Ip}{2I+1}\sum_j b_{ij}^2. \tag{21}$$

All of Eq. (18) may, therefore, be treated as in (20), with the result that

$$M_2=23.4\frac{g_S^2\mu_0^4}{\hbar^2a^6}\left[\frac{4}{9}D(D+1)g_I^2+\frac{1}{9}\frac{8I+9}{2I+1}g_S^2p\right]. \tag{22}$$

If this equation is rewritten in terms of Gauss, there results

$$[\langle\Delta H^2\rangle_{\mathrm{av}}]^{1/2}=\left[\frac{\hbar^2M_2}{g_S^2\mu_0^2}\right]^{1/2} =1.61\frac{\mu_0}{a^3}\left[4D(D+1)g_I^2+\frac{8I+9}{2I+1}S(S+1)g_S^2p\right]^{1/2}. \tag{23}$$

If only the nuclear spins were effective in broadening the lines, the rms linewidth would be on the order of a gauss. Even small concentrations of unpaired atoms will mask the nuclear effects, however; for concentrations of 10 to 100 D atoms per million lattice sites, the rms linewidth will range between 2.1 and 6.6 G.

The expressions for the fourth moment of the line are very complicated and will not be dealt with in full. The result obtained by Kittel and Abrahams for random population by a single species of spin cannot be very misleading if applied here, and it will be adopted without change. If the contributions from the nuclear moments are neglected, the fourth moment will be

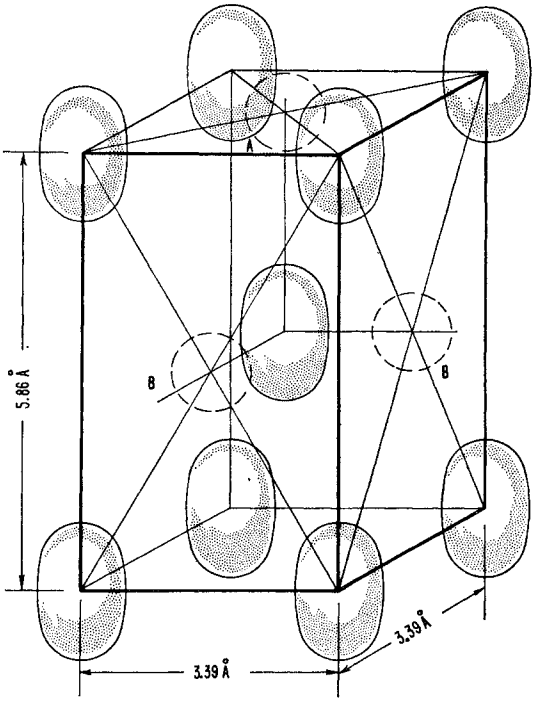

FIG. 7. Sketch of the lattice of solid D_2.

$$M_4=3(\langle\Delta\omega^2\rangle_{\mathrm{av}})^2\left[0.742+\frac{1}{p}\left\{0.098-\frac{0.021}{S(S+1)}\right\}\right]. \tag{24}$$

The value which would be obtained from a rigorous calculation of the fourth moment will lie somewhere between the value obtained by using the true second moment (22) in (24) and the value obtained by using a second moment computed by ignoring the splitting arising from the hyperfine interaction [i.e., which would be obtained by setting $I=0$ in (22)]. For $p=10^{-5}$ and $p=10^{-4}$ the root-mean quartic (rmq) linewidths will lie between 25 and 32 G and between 45 and 56 G, respectively.

In calculating the nuclear contribution to the rms linewidth it was assumed that the atoms occupied substitutional positions in the lattice. If the atoms all occupied interstitial positions instead, the nuclear contributions could be several times larger. The matter is not an academic one, since the rms linewidths will be substantially those due to the nuclei for values of p below 10^{-6} or 10^{-7}, a condition accessible to observation during the early part of each experimental run. Table I compares the nuclear contribution to the rms and rmq

TABLE I. Line parameters for the case of extreme atomic dilution.

Lattice site	$[\langle\Delta H^2\rangle_{\mathrm{av}}]^{1/2}$ (G)	$[\langle\Delta H^4\rangle_{\mathrm{av}}]^{1/4}$ (G)	$[\langle\Delta H^4\rangle_{\mathrm{av}}/\langle\Delta H^2\rangle_{\mathrm{av}}^2]^{1/2}$
Substitutional	0.40	0.52	1.30
Interstitial at A	0.81	1.00	1.26
Interstitial at B	1.50	1.74	1.13

[12] V. W. Kogan, B. G. Lazarev, and R. F. Bulatova, Zh. Eksperim. i Teor. Fiz. **37**, 678 (1959) [translation: Soviet Phys.—JETP **10**, 485 (1960)].

[13] C. Kittel and E. Abrahams, Phys. Rev. **90**, 238 (1953).

moments for substitutional sites with those arising through occupation of the two interstitial sites defined in Fig. 7. The dimensions a and c of the body-centered tetragonal unit cell were taken[12] as 3.39 and 5.86 Å, respectively. The rmq moments were calculated from the expression[14]

$$H_{\text{nuc}}{}^{4\,1/4}=\tfrac{2}{3}g_I\mu_0[D(D+1)]^{1/2}\Big[\frac{2}{3}\sum_{j>j'}b_{ij}{}^2b_{ij'}{}^2+\frac{1}{5}\frac{D(D+1)-\frac{1}{3}}{D(D+1)}\sum_j b_{ij}{}^4\Big]^{1/4}$$
$$=\tfrac{2}{3}g_I\mu_0[D(D+1)]^{1/2}\Big[\frac{81}{48}\{\sum_j(\tfrac{2}{3}b_{ij})^2\}^2-\frac{2D(D+1)+1}{15D(D+1)}\frac{81}{16}\sum_j(\tfrac{2}{3}b_{ij})^4\Big]^{1/4}. \quad (25)$$

All lattice sums were adjusted to account for the fact that, in thermodynamic equilibrium at helium temperatures, one molecule in six is nonmagnetic, being in a nuclear spin $D=0$ state. The remaining molecules will have $D=2$, all but a fraction of a percent of the molecules being in the *ortho*-state with rotational angular momentum zero.

Saturation

When any one of the transitions of Fig. 6 is strongly excited, the populations of the energy levels will deviate from the Boltzmann distribution characteristic of thermodynamic equilibrium. When the source of excitation is removed, the density matrix of the atomic system will return to its earlier form in a way characteristic of the interaction of the atoms with the lattice. It will be assumed here that the off-diagonal elements of the atomic density matrix all vanish. The relaxation of the populations of the N-atomic energy levels will then be described by a set of N-linear rate equations. There will be six such equations for the system of Fig. 6, five of which are linearly independent. If the energy levels are numbered clockwise beginning at the uppermost level, the rate equations for the relaxation may be written

$$\frac{d}{dt}\begin{pmatrix}N_1\\N_2\\N_3\\N_4\\N_5\\N_6\end{pmatrix}=\begin{pmatrix}-(Q+BR) & Q & 0 & 0 & 0 & R\\ Q & -(2Q+BP+BR) & Q & 0 & R & P\\ 0 & Q & -(Q+BP+BR) & R & P & 0\\ 0 & 0 & BR & -(Q+R) & Q & 0\\ 0 & BR & BP & Q & -(2Q+P+R) & Q\\ BR & BP & 0 & 0 & Q & -(Q+P+R)\end{pmatrix}\begin{pmatrix}N_1\\N_2\\N_3\\N_4\\N_5\\N_6\end{pmatrix}. \quad (26)$$

It has been assumed that only the "allowed" and "first-forbidden" transitions are of any importance in the relaxation, and in the interests of simplicity the possibility of allowed nuclear-quadrupole relaxation connecting levels 1 and 3 or levels 4 and 6 has been excluded. The coefficient B in the relaxation matrix is a Boltzmann factor, $B=\exp(g_S\mu_0H/kT)$. The small contribution of the hyperfine energy to B has been neglected.

In our experiments it was apparent that Q processes played an important, if not dominant role in relaxation. If P and R are negligible with respect to Q, the behavior of the populations after a brief microwave pulse sufficient to saturate the $(-\frac{1}{2},1)\leftrightarrow(\frac{1}{2},1)$ transition will be

$$\begin{aligned}N_1(t)&=1-N_6(t)=\tfrac{1}{6}+\tfrac{1}{4}e^{-Qt}+\tfrac{1}{12}e^{-3Qt},\\ N_2(t)&=1-N_5(t)=\tfrac{1}{6}-\tfrac{1}{6}e^{-3Qt},\\ N_3(t)&=1-N_4(t)=\tfrac{1}{6}-\tfrac{1}{4}e^{-Qt}+\tfrac{1}{12}e^{-3Qt}.\end{aligned} \quad (27)$$

Equations (27) may be expected to describe the initial readjustments of the populations if the hyperfine sublevels of either Zeeman multiplet tend to reach equilibrium with each other more rapidly than with the states of the other multiplet.

[14] Ref. 10, Eq. (29).

A more familiar special case is that in which $Q=P=0$. Equation (26) decomposes into three pairs of equations, each of which describes relaxation in the two-level system, $(I_z',\frac{1}{2})\leftrightarrow(I_z',-\frac{1}{2})$. The vertical relaxation between the two levels is characterized by a single exponential having characteristic time $(2R)^{-1}$.

Saturation

It is necessary to add another term to (26) to describe the behavior of the system while external microwave or rf fields are being applied. If, for instance, the $(-\frac{1}{2},1)\leftrightarrow(\frac{1}{2},1)$ transition is steadily driven, the required term will be

$$\frac{d}{dt}\begin{pmatrix}N_1\\N_2\\N_3\\N_4\\N_5\\N_6\end{pmatrix}=\begin{pmatrix}-W & 0 & 0 & 0 & 0 & W\\ 0 & 0 & 0 & 0 & 0 & 0\\ 0 & 0 & 0 & 0 & 0 & 0\\ 0 & 0 & 0 & 0 & 0 & 0\\ 0 & 0 & 0 & 0 & 0 & 0\\ W & 0 & 0 & 0 & 0 & -W\end{pmatrix}\begin{pmatrix}N_1\\N_2\\N_3\\N_4\\N_5\\N_6\end{pmatrix}, \quad (28)$$

where W is the microwave-induced transition proba-

bility. The following set of equations, obtained from (26) and (28) by setting $N_4=1-N_1-N_2-N_3-N_5-N_6$, may be used to describe the populations in the steady state:

$$\begin{bmatrix} 0 \\ 0 \\ -R \\ -Q \\ 0 \end{bmatrix} = \begin{bmatrix} -(Q+BR+W) & Q & 0 & 0 & R+W \\ Q & -(2Q+B(P+R)) & Q & R & P \\ -R & Q-R & -(Q+BP+(B+1)R) & P-R & -R \\ -Q & BR-Q & BP-Q & -(3Q+P+R) & 0 \\ BR+W & BP & 0 & Q & -(Q+P+R+W) \end{bmatrix} \begin{bmatrix} N_1 \\ N_2 \\ N_3 \\ N_5 \\ N_6 \end{bmatrix} \tag{29}$$

Because the parameter W in these equations can be made arbitrarily large, this system is more tractable by approximations than is (26). If Q is large compared to P and R, a good approximation to the determinant Δ of coefficients in (29) is obtained by retaining only the terms in WQ^4 and WQ^3:

$$\Delta \xrightarrow[W\to\infty]{} 6Q^4W-Q^3W[(9+15B)P+18(1+B)R]. \tag{30}$$

The intensity of the microwave resonance line will be proportional to (N_6-N_1). By retaining only terms in Q^4 and Q^3 in the expansion of determinants, one finds according to Cramer's rule that

$$(N_6-N_1) \xrightarrow[W\to\infty]{} \left[3R+2P-\frac{1}{Q}(12R^2+16RP+6P^2)\right] \times\frac{(N_6-N_1)_0}{W}, \tag{31}$$

where $(N_6-N_1)_0$ is the population difference in the absence of externally applied microwave fields. Had only terms in Q^4 been retained in the calculation, the result would have been

$$(N_6-N_1) \xrightarrow[W\to\infty]{} [(3R+2P)/W](N_6-N_1)_0,$$

which could have been written down immediately under the assumption that the Q relaxation maintained the hyperfine sublevel populations in equality with one another at all times.

A similar analysis of the behavior of the $(-\frac{1}{2}, 0) \leftrightarrow (\frac{1}{2},0)$ transition results in the expression

$$(N_5-N_2) \xrightarrow[W\to\infty]{} \left[\frac{3R+2P-(1/Q)(8R^2+8RP+2P^2)}{W}\right] \times(N_5-N_2)_0. \tag{32}$$

A much simpler analysis gives, for the case $Q=0$, the result

$$\Delta N \xrightarrow[W\to\infty]{} (R/W)(\Delta N)_0, \tag{33}$$

where ΔN may be either (N_6-N_1), (N_5-N_2), or (N_4-N_3). The three transitions behave identically under extreme saturation.

EXPERIMENTAL RESULTS

Buildup of Unpaired Atoms

Once a tritiated sample was frozen, the growth of the concentration of unpaired atoms proceeded at a rapid rate. Three strong atomic resonances in the neighborhood of 8600 G were observable within seconds after the completion of the condensation and could be displayed without narrow banding. These resonances occurred at very nearly the field values predicted for the three allowed transitions of free atomic deuterium.

The concentration of unpaired atoms was studied over a period of days by sweeping the magnetic field back and forth through the resonances and photographing the oscilloscope tracing of the second detector output.

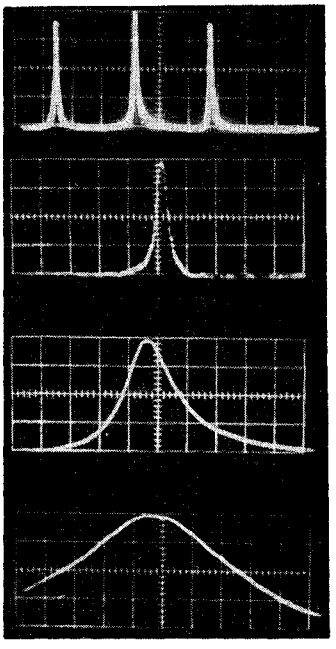

FIG. 8. Typical oscilloscope displays. Above: The 3 D lines at 4.2°K and sample age 23 min. Peak spacing is 78 G. Below: high-field D line at fivefold sweep magnification. Sample ages 12 min, 6 days, and 6 days. In bottom oscillograph $T=1.2°$.

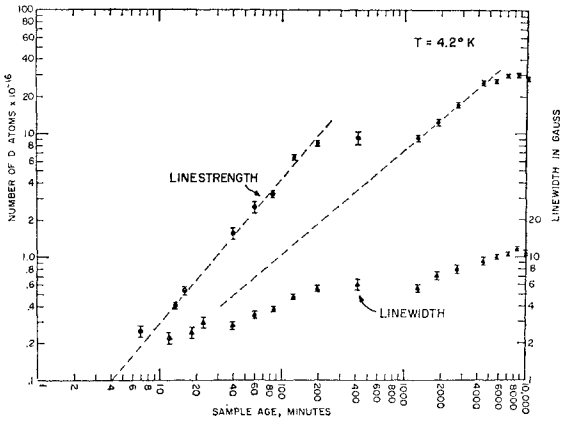

FIG. 9. Growth of atomic concentration and line breadth.

Typical traces appear in Fig. 8. The abscissas are roughly linear in the external magnetic field, the ordinates being proportional to the absorption component of the sample resonance. The peak intensities of the lines failed to increase in proportion to the time elapsed after freezing, and their widths increased slowly. Figure 9 displays the fullwidth at half-intensity and the approximate integrated strength, obtained by multiplying the peak intensity by the half-width, of the high-field D line as a function of the age of the sample. The sample contained about 400 cm³ (NTP) of deuterium gas and 4 cm³ (NTP) of tritium gas. The indicated errors in the points labeled "line strength" arise chiefly from errors in the measurement of the half-width. These points were not corrected for the changes in the functional form of the line shape which occurred during the aging of the sample.

The most striking feature of the data of Fig. 9 is the plateau between the initial linear growth of the atomic concentration and the subsequent regrowth to the steady values achieved after about seven days of storage at 4.2°K. Since the energy released per unit time by tritium decays is constant as far as this experiment is concerned, the appearance of the plateau was unexpected. Although the plateau is doubtlessly exaggerated by the crude way in which the linestrength was computed, the linewidth data also have a plateau, and a satisfying interpretation of its presence must be sought more deeply.

An incisive explanation for the plateau was provided when the absorption curve *derivatives* were recorded by means of the 30 cps modulation and synchronous detection equipment (Fig. 2). Figures 10–12 show the derivatives of the high-field D absorption observed at sample ages of 2 h, 24 h, and 7 days, all observed during a single run and recorded at the same gain and microwave power level. The double hump on each side of the tracing of Fig. 12 is quite unusual, and suggests that the resonance line is a composite one in which the peaks of a narrow line and a broad line coincide. This interpretation is strengthened by the other two figures, which show the broad component only as unresolved shoulders of increasing magnitude upon the derivative of the narrow component, whose amplitude has not changed from one tracing to the next. The broad component must, therefore, build up much more slowly in time than the narrow component, which has reached its full strength within a few hours of the time at which the sample was frozen. The plateau of Fig. 9 is produced when the concentration of atomic centers responsible for the narrow component reaches its saturation value. The time at which this occurs is about 200 min after freezing, according to Fig. 9, and this value is consistent with the equality of the derivative amplitudes in Figs. 10–12. The "regrowth" is due to the continued buildup of the broadline centers, which reach a saturation concentration after about 8500 min.

The relative growth rates may be determined from the initial slopes of the growth and regrowth regions; the rate of production of the broad line centers is only about 9% that of the narrow line centers. The lines which best fit the linear portions of the growth and regrowth regions intersect, when extrapolated, at time 0.8 min and $N=0.02$, which strongly suggests that the broad line component, like the narrow line component, begins to build up at $t=0$. The broad line centers thus do not arise from a "phase transition" which occurs when some critical concentration of atomic centers is reached.

Not shown on Fig. 9 are two pairs of resonances which

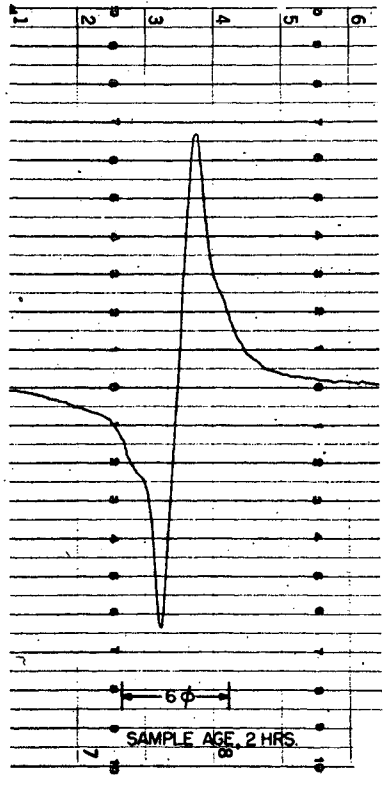

FIG. 10. Derivative of the absorption component of the high-field D line. Sample age, 2 h. The symbol ϕ is used to mean Gauss. The magnetic field increases towards the right.

correspond very closely to those expected for free atomic tritium and atomic hydrogen. These became visible photographically about an hour after condensation. The tritium atom concentration reached a saturation value after 4 or 5 days of about 1.1% of the total concentration of atomic deuterium, which agrees well with the composition of the sample. Both the growth curves and the microwave resonances (Fig. 13) of the T and H atoms are simple.

The Microwave Susceptibility and Number of Spins

The atomic resonances were so strong that it was a fairly simple matter to make an absolute measurement of the susceptibility of the sample at microwave frequencies. The method compared the change brought about by atomic absorption in the microwave power reaching the mixer crystal M_1 with an equivalent change brought about by altering the amplitude of the microwave carrier incident upon the cavity. The atomic absorption will produce a change

$$I_{\text{s.d.}}=-2\pi\eta sAQ_L(1-\Gamma_{\text{res}}^2)\chi'' \tag{34}$$

in the signal current at the second detector, where η is the filling factor of the sample, Q_L is the loaded Q of the cavity, $2^{1/2}A$ is the amplitude of the microwave carrier incident upon the cavity, Γ_{res} is the reflection coefficient of the cavity at exact resonance, and χ'' is the absorptive component[15] of the microwave susceptibility of the sample. The factor s contains the gain of the i.f. strips and the conversion efficiency of the mixer and second detector. If the balance arm of the microwave bridge is completely matched, a change in the setting of attenuator A_2 will produce a change of

$$I_{\text{s.d.}}=\alpha sA\Gamma_{\text{res}}. \tag{35}$$

Here $(1+\alpha)$ is the ratio of carrier amplitude after resetting to that before resetting.

The unknown quantities s and A will cancel when (34) and (35) are equated, and the measurement will thus give an absolute determination of χ''. The result is independent of the conversion characteristic of the mixer crystal. The attenuators were calibrated *in situ*, at the resonance frequency of the sample cavity, by a bolometer bridge. The Q_L of the cavity and the value of Γ_{res}^2 were measured with a crystal which was known to be operating in the square-law region.

The microwave susceptibility χ'' is related[15] to the number of spins in the sample by

$$\chi''=\tfrac{1}{2}\pi N\omega_0\frac{g s^2\mu_0^2S(S+1)}{3kT}f(\omega). \tag{36}$$

Here N is the number of spins per unit volume which participate in the transition in question, S is the total electronic spin (which has the value $\frac{1}{2}$ in these experiments), ω_0 is the resonance frequency, k is Boltzmann's constant, 1.38×10^{-16} erg/molecule/deg, and T is the absolute temperature. The function f is the line profile introduced in Eq. (17). If (35) and (34) are equated and the result combined with (36) and with (1), there results

$$\mathfrak{N}=\frac{-\alpha\Gamma_{\text{res}}V_{\text{cavity}}}{0.54\pi^2Q_L(1-\Gamma_{\text{res}}^2)[g s^2\mu_0^2S(S+1)/3kT]H_0f(H)}, \tag{37}$$

where now $f(H)$ is the line profile normalized to unity in units of magnetic field and $\mathfrak{N}=NV_{\text{sample}}$ is the total number of spins participating in the resonance.

The principal difficulty in the measurement of $\mathfrak{N}$ is the choice of a tractable functional form for the reso-

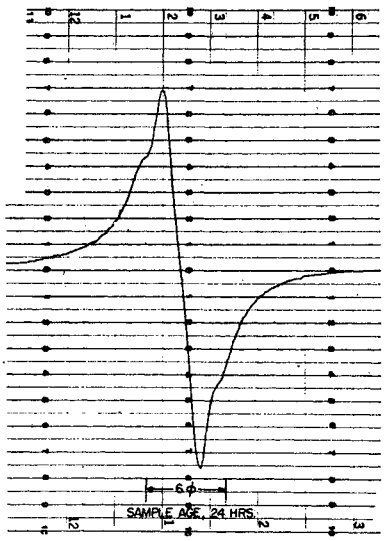

FIG. 11. Derivative of the absorption component of the high-field D line. Sample age, 24 h. The magnetic field increases towards the left.

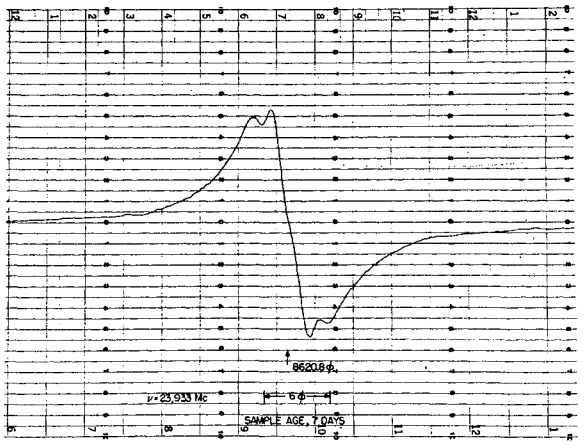

FIG. 12. Derivative of the absorption component of the high-field D line. Sample age, 7 days. The magnetic field increases towards the left.

[15] N. Bloembergen, E. M. Purcell, and R. V. Pound, Phys. Rev. 73, 679 (1948).

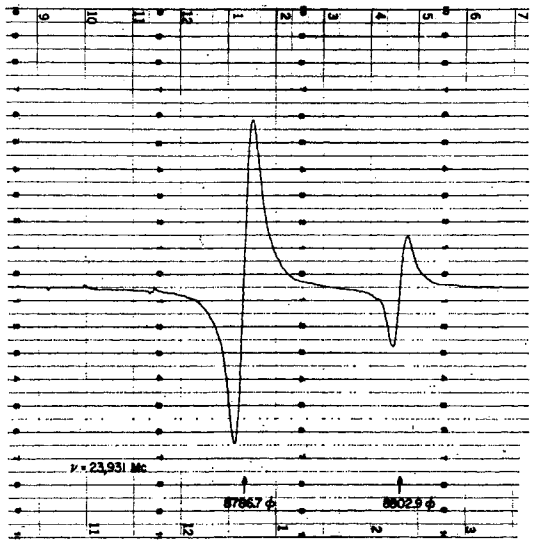

FIG. 13. Derivatives of the absorption components of the high-field T and H lines. The T line is the weaker.

nance profiles. The Lorentzian is an appropriate, if approximate, form for the D-atom resonances in old samples, and the function $f(H)$ was taken to be

$$f(H)=\frac{1}{\pi\delta H}\frac{1}{1+((H-H_0)/\delta H)^2}, \tag{38}$$

with half-width δH at half-intensity equal to 5.4 G, as required by Fig. 9. The value of $f(H)$ at line center is then 0.059 G^{-1}.

The deflection of the microammeter at the second detector produced at the peaks of the D-atom absorptions in a sample seven days old was found equal to the deflection produced by an increase of $\alpha=0.175$ in the amplitude of the microwave carrier when the magnetic field was set far from the resonant values. The balance arm of the microwave bridge was well matched in both cases, as could be checked by connecting a matched load to the sample arm of the bridge. This value of α, together with the cavity parameters $Q_L=10\,000$, $\Gamma_{res}=-0.44$, and $V_{cavity}=4.33$ cm^3, leads to a value of 1.04×10^{17} for the number of electron spins participating in each allowed D-atom transition. The total number of spins in the sample was therefore 3.1×10^{17}. It is this value which has been used to label the "number of G atoms" scale in Fig. 9. We have some reasons to believe that the correct value of Γ_{res} might have been smaller by a factor as large as 2 than our measured value; our value for the total number of spins may therefore be a factor of 2 too large.

With the numerical scale thus established, it becomes possible to verify that the growth in atomic concentration is rather spectacular. The growth curve shows that unpaired atoms were being created at a net rate of 8.2×10^{12}/sec. The total activity of the 4 cm^3 of tritium which the deuterium contains is 10.4 C, or 3.7×10^{11} disintegrations per second. Each tritium decay, therefore, produces, on the average, 22 unpaired atoms. Since the average energy of the beta particle emitted in the decay is 5.69 keV,[16] the total energy available per second from the tritium decays is 2.1×10^{15} eV/sec. It requires about 11.5 eV to dissociate an H_2 molecule by electron bombardment,[17] so that a minimum of 4.7×10^{13} eV/sec is expended in producing atomic centers at the observed net rate, which corresponds to utilization of 2.2% of the available energy.

It follows that at least 2.2% of all the tritium, and therefore 2.2% of the total gas sample, must actually have condensed into the cavity at the time of freezing. If it be assumed that all of the sample was actually deposited in the cavity, the 3.1×10^{17} unpaired atoms would then correspond to an average concentration of 33 atoms per million lattice sites. The effective energy dose per atom produced would be 95 eV/atom. The strength of the D_2 nuclear magnetic resonance signals, as measured against the shunt conductance calibrator[18] of our marginal oscillator, and the number of electron spins, as measured by the technique described, having varied by factors as large as 2 from run to run, it is doubtful that all the sample was ever condensed successfully into the cavity. The values just obtained for the atomic concentration and dissociation dosage must therefore be regarded as lower and upper limits, respectively. They are, nonetheless, at rather serious variance with the conclusions drawn from two previous investigations of radiation damage in solid hydrogen. In the earlier of these, solid H_2 at 4.2°K was bombarded[19] with 40-MeV electrons from a linear accelerator. A production of 0.2 atom per 100 eV of energy absorbed in the sample was reported, which is only one-fifth or less of the figure obtained here. In another investigation more similar to that reported here, the effect of the self-damage produced by tritium decay in solid T_2 was assessed by studying first pure tritium and then tritium mixed with neon.[20] It was concluded that unpaired T atoms were produced only by the decay of T_2 into T+He^3, and that the energy carried off by the beta particle did not produce further dissociation of T_2. Thus, only one unpaired atom would have been produced per tritium decay.

A few experimental details should be offered in support of the growth data of Fig. 8, which must implicitly reflect instability in the gains of the i.f. strips from hour to hour and day to day. These variations were compensated by resetting the gain controls so that at given settings of the attenuators in the local oscillator and

[16] G. H. Jenks, J. H. Sweeton, and J. A. Ghormley, Oak Ridge National Laboratory Report, ORNL 333, 1960 (unpublished).

[17] H. S. W. Massey and E. H. S. Burhop, *Electronic and Ionic Impact Phenomena* (Oxford University Press, New York, 1956).

[18] G. D. Watkins, thesis, Harvard University, 1952 (unpublished).

[19] L. H. Piette, R. C. Rempel, H. E. Weaver, and J. M. Flournoy, J. Chem. Phys. **30**, 1623 (1959).

[20] John Lambe, Phys. Rev. **120**, 1208 (1960).

signal klystron paths, the current at the second detector was always 20 μA. The average power outputs of the klystrons were stable within several percent from day to day, for the dc currents at M_1, M_2, and M_3 were quite reproducible.

Properties of Young Samples

The plateau of Fig. 8 conveniently separates the microwave susceptibility of the sample into two regions. In samples less than four or five hours old, the response to microwave excitation will be overwhelmingly determined by atoms in narrow line sites. In the older samples in which the broad line centers predominate, the resonance properties will be determined primarily by the broad line sites. The temporal separation of the two regions makes possible, in effect, separate study of two sites which have coincident spectra.

Measurement of Effective g and A Values

Since it required only about an hour to measure accurately the field positions of the atomic resonances, the effective spectroscopic splitting factor, g, and the effective hyperfine-coupling constant, A, were easily determined for samples less than 4-h old. Before a sample was warmed and recondensed for such a determination, all equipment had been turned on and running for six to eight hours. The temperatures of the magnet yoke and of the air surrounding the spectrometer had thus had time to come to steady values. The detailed shape of the magnetic field and the calibration of the microwave wavemeter could be then assumed constant.

The magnetic field setting of each resonance was determined by displaying the derivative of its absorption component, obtained by a small 30 cps modulation of the field, and that of the nuclear resonance of Li^7 nuclei in a liquid sample outside the cryostat, together on a dual channel oscilloscope whose horizontal plates were driven by the modulation generator. Because the derivatives vary rapidly about line center, very accurate location of the ESR peaks could be effected by requiring simultaneous null of the ESR and the Li^7 derivatives. Every effort was made to ensure that the microwave bridge was balanced to suppress completely the dispersive component of the resonance, whose presence would introduce asymmetry into the line shape. The centers of the D lines could thus be located to within 0.075 G, or roughly 0.014 half-widths. The T lines were much weaker and noisier, and their peaks could only be located within 0.20 G, or about 0.04 linewidth.

When the frequency of the Harvey-Wells, Inc., marginal oscillator used to monitor the Li^7 resonance had been adjusted to produce simultaneous null of the two derivative signals, it was measured against the fourth harmonic of a U. S. Navy Bureau of Ships LM-18 heterodyne frequency meter, which could be calibrated against its own internal crystal. The crystal resonated at $1\,000\,000\pm10$ cps. The frequencies were compared by observing the beats on the output of the Harvey-Wells unit, which was coupled radiatively to the heterodyne frequency meter. The Harvey-Wells unit oscillated rather "hard," and no pulling of its frequency was apparent. The beat frequency would often drift slowly through zero. The frequencies could be compared to within 60 cps, so that the frequency of the Li^7 resonance was determined to within $4\frac{1}{2}$ ppm.

The major error in our spectroscopic endeavors lay in the determination of the frequency of the microwave carrier. For this purpose we used an ordinary tunable absorption cavity wavemeter, which we calibrated both before and after our experiments against the well-known inversion spectrum[21] of the NH_3 molecule. The strong lines at 23 870 and 24 139 Mc/sec were quite close to the resonant frequency of the sample cavity. The klystron frequencies could, over this range, be measured to within ±2 Mc/sec, these errors reflecting parallax in the fiducial system of the wavemeter. The resettability of the wavemeter appeared to lie within these limits, and the two calibration runs gave results which differed by 1 Mc/sec. Wavemeter reading corrections accounting for changes in ambient temperature and humidity were less than 0.3 Mc/sec in magnitude.

When the measurement of a given line had been completed the field was moved to the position of the next resonance desired, going systematically from the lowest value to the highest value, or *vice versa*. The changes were made very slowly in order to avoid local heating of the magnet pole caps or yoke by eddy currents. Since the resonance frequency of the sample cavity varied a megacycle or two with the field setting (there was a broad-background resonance, undoubtedly in the teflon coil form, centered about $g=2$), the microwave carrier frequency was read for each resonance while the field was set at the peak of that resonance. When all the resonances had been measured, the cryostat was removed from the magnet gap and the magnetic field mapped by moving the Li^7 sample back and forth in the gap, the magnetizing current remaining fixed. The corrections from Li^7 resonance frequency at the monitor position to the Li^7 frequency at the position occupied by the sample cavity, when in normal location, varied between -19 and -17 parts per 100 000 of the monitor frequency.

The values of g and A were computed with the aid of the following values for the Bohr magneton and gyromagnetic ratios of the various nuclides[22–26]:

---

[21] C. H. Townes and A. L. Schawlow, *Microwave Spectroscopy* (McGraw-Hill Book Company, Inc., New York, 1955).
[22] J. H. Gardner, Phys. Rev. **83**, 996 (1951).
[23] H. A. Thomas, R. L. Driscoll, and J. A. Hipple, Phys. Rev. **78**, 787 (1950).
[24] G. Lindström, Arkiv Physik **4**, 1 (1952).
[25] T. F. Wimett, Phys. Rev. **91**, 499A (1953).
[26] Hans Kopfermann, *Kernmomente* (Akademische Verlagsgesellschaft, Frankfurt A/M, 1956), p. 441.

$$\mu_{\text{proton}} = (1.52101 \pm 0.00002) \times 10^{-3} \mu_0 ,^{22}$$

$$\gamma_{\text{proton}} = \frac{2}{\hbar} \mu_{\text{proton}} = (2.67528 \pm 0.00006) \times 10^4 \text{ sec/G} ,^{23}$$

$$\gamma(\text{Li}^7)/\gamma(H^1) = 0.3886341 \pm 0.0000010 ,^{24}$$

$$\mu_D/\mu_H = 0.307012192 \pm 0.000000015 ,^{25}$$

$$\mu_T/\mu_H = 1.06664 .^{26}$$

The results obtained from a four-hour old sample are listed in Table II. These results are in good agreement with several less precise measurements made on other young samples.

Shape and Width of the Resonance Lines

When first observable, the atomic deuterium resonance lines have, at 4.2°K., a peak which is Gaussian in appearance (Fig. 8) and which has a full width at half intensity of 2.2±0.2 G. The wings of the line become more pronounced within a few minutes, but the width of the lines increases only slowly. While the sample age increases from 12 to 40 min, the number of atomic centers increases by a factor of 3.3 but the half-width increases by only 30%. The initial peak must, therefore, represent the form which the resonance curve would have in the limit in which the average concentration of the atomic centers goes to zero; i.e., it must represent the broadening arising solely from the molecules in the vicinity of a typical atomic site.

That this broadening arises from nuclear moments rather than from a distribution of orbitally inequivalent lattice sites may be deduced from the symmetry and equivalence (apart from the background resonance in the teflon) of the three D lines. The lines therefore originate from atoms in a single type of lattice site, which may perhaps be identified directly by its line breadth. Let the resonance lines in very young samples be represented by a Gaussian curve having a full width at half-maximum intensity of 2.2±0.2 G. Let the wings of the actual resonances, which are not characteristic of a Gaussian, be ascribed to residual interaction of each atom with the other atoms in the sample. If the wings are dropped from consideration and attention focused only on the neighborhood of the peak, the second moments of the resonance curves will be $(2.8 \pm 0.5) \times 10^{14}$ sec^{-2} and the rms linewidths will be 0.94±0.09 G. If one accepts the view that the lattice in the locale of the atomic centers is like the deuterium lattice observed in x-ray diffraction studies,[12] then he is led rather forcefully to identify the sites occupied by the D atoms in the very youngest of samples as type *A* interstitials (Table I).

An unexpected property of the D-atom resonances in young samples became evident during some transient saturation studies. If the line breadths arose from variations in the local magnetic field from site-to-site, the lines should be inhomogeneously[15,27] broadened, and it should be possible to "burn a hole"[15] in each of the lines by saturating it in one position. Alternatively, if the line is swept through rapidly at microwave intensities sufficient to saturate it during the time of passage, then the line shape should differ only in its amplitude and apparent half-width from the unsaturated line. The saturating passage through the peak of the resonance line should not affect the behavior of the wing swept through subsequently, and thus the two wings of a symmetrical unsaturated line should remain mirror images of each other, even under extreme saturation.

Such was not the case for the resonances observed in these samples. Not only does passage through the peak, where transition probabilities are highest, severly reduce the intensity of the following wing, but the point at which the microwave-induced transition probability overwhelms the relaxation mechanisms moves towards the initial wing as the power level is raised. The resonance lines are *homogeneously* broadened.

Relaxation

The spin-lattice relaxation time, T_1,[15] of the D ESR signals was studied by executing a pair of saturating passages in succession. The relative amplitude of the signal observed on the second passage is a measure of the recovery of the electronic polarization during the interval between the two passages. After several relaxation times had elapsed, the sequence was re-executed, a different time interval separating the two passages. The passages were programmed by driving the magnet power supply by a triangular voltage waveform from a Hewlett-Packard Model 202A function generator.

Plots on semilogarithmic graph paper of the fractional recovery against elapsed time interval were linear within estimated experimental error, so that the recovery is characterized, to good approximation, by a single exponential. The characteristic time of the exponential varies from 0.440±0.030 sec for a 32-min old sample having linewidths of 2.8 G to 0.220±0.025 sec for a 200-min old sample having linewidths of 5.6 G. The relaxation time varies inversely with linebreadth during this period, and remains at 0.20 to 0.22 sec throughout the plateau region of the growth curve. The behavior in the regrowth region is more complicated and will be discussed later.

TABLE II. Effective g and A values for young sample.

Atomic species	Transition	Experimental data corrected Li^7 NMR frequency (Mc/sec)	Klystron frequency (Mc/sec)	Spectroscopic splitting factor and hyperfine coupling constant (Mc/sec)
Deuterium	$I_z' = 1$	14.01065	23 948	$A = 218.86 \pm 0.15$
	−1	14.27104	23 947	$g = 2.0022 \pm 0.00016$
	0	14.14140	23 948	$g = 2.0022 \pm 0.00016$

[27] A. M. Portis, Phys. Rev. 91, 1071 (1953).

Saturation

It is of interest to study the behavior of the ESR signals under steady saturation, thereby obtaining a value of the relaxation time which is experimentally independent of that measured by the rapid passage technique. Saturation curves were obtained by coordinating attenuators A_2 and A_4 in the familiar manner. The second detector signal, $\delta I_{\text{s.d.}}$, would be independent of the setting of A_2 as long as the resonance were not saturated, but would diminish without limit as the microwave power level increased into the saturation region. Figure 15 shows typical signals observed as a function of the inverse of the microwave power incident upon the sample. The saturation region at the left of the plot may be well fitted by a straight line.

Once the parameter W has been related to the power incident upon the cavity, the parameter R can be determined from Eq. (33). We have for the average rf energy stored in components perpendicular to the external field the expression

$$\langle \hat{H}_1^2 \rangle_{\text{sample}} = \frac{8\pi\eta Q_L(1-\Gamma_{\text{res}}^2)}{\omega_0 V_{\text{sample}}} P_0 = \frac{4.3\pi Q_L(1-\Gamma_{\text{res}}^2)}{\omega_0 V_{\text{cavity}}} P_0, \quad (39)$$

where P_0 is the incident power. The transition probability W, when averaged over the sample, becomes, from standard time-dependent perturbation theory,

$$\langle W \rangle_{\text{sample}} = \frac{2.2^2 Q_L(1-\Gamma_{\text{res}}^2) P_0}{V_{\text{cavity}}} \frac{f(H)}{H_0}, \quad (40)$$

so that one finds from the numerical values listed earlier the relation

$$\langle W \rangle_{\text{sample}} = 0.51 P_0, \quad (41)$$

with P_0 in ergs/sec. From data on a sample four hours old, one finds from (33) that $T_1^{\text{sat}} \equiv (2R)^{-1} = 0.095$ sec, which is about half the measured value of T_1.

It is puzzling that the steady state saturation data should predict a relaxation time which is *shorter* than that observed by the fast passage saturation-recovery technique, and the various corrections which might be imagined for the calculation of (41) all decrease further the value of $(2R)^{-1}$. Thus, if the Q_L of the cavity had been somewhat underestimated (the value of 10 000 was a lower limit set by the resolution of the wavemeter), the correction would decrease $(2R)^{-1}$. Corrections accounting for the possibility that the ESR lines contain a trace of inhomogeneous broadening would do likewise. The power values were based upon an absolute measurement with a bolometer bridge and are probably reliable. We are thus for the present confronted with a mystery, to which we shall return in due course.

Properties of Well-Aged Samples

Effective g and A Values

The interpretation of the spectral data for older samples is complicated by the composite nature of the D-atom resonances, as illustrated by Fig. 12. It is evident that the two peaks are very slightly displaced from one another, the peak of the broader component falling at a slightly lower field value than that of the narrow component. The displacement is perhaps $\frac{1}{2}$ G, and is doubtless responsible for the wiggle about the center of inversion of the tracing. The low-field line shows the same effect, while the component separation in the case of the mid-field line is somewhat smaller. The g and A values of the two components thus differ by less than 1 part in 10^4. Approximate values for the composite lines are presented in Table III. The values may be compared with the g value of the free atomic species,[28] 2.002256, and the free atomic hyperfine coupling constants $A_D = 218.25623$ Mc/sec,[29] $A_T = 1516.70147$ Mc/sec,[30] and $A_H = 1420.40575$ Mc/sec.[30]

Shape and Width of the Resonance Lines

At 4.2°K, the D-atom resonances in well-aged samples appear Lorentzian, with a full width at half-intensity of 10.8 G. If a full cutoff width of 80 G (roughly the spacing between adjacent D lines) is selected to make the moment calculations converge,[31] the estimated rms and rmq linewidths are $M_2^{1/2} = 11.7$ G and $M_4^{1/4} = 29.4$ G, which disagree rather sharply with the estimates based on the Kittel-Abrahams theory. The disagreement might be substantially lessened by choosing a larger cutoff width and assuming atomic concentrations substantially in excess of 100 per million lattice sites.

Such an effort does not seem justified, however. Since the broad wings of the Kittel-Abrahams line result from a small number of pairs of atoms which lie very close together, the choice of a cutoff width corresponds to a choice of the distance of closest approach. The choice of 80 G corresponds to a minimum distance of about

TABLE III. Effective g and A values for old sample.

Atomic Species	Transition	Experimental data corrected Li^7 NMR frequency (Mc/sec)	Klystron frequency (Mc/sec)	Spectroscopic splitting factor and hyperfine coupling constant (Mc/sec)
Deuterium	$I_z' = 1$	14.00945	23 942	$A = 218.08 \pm 0.15$
	-1	14.26820	23 944	$g = 2.0019 \pm 0.00017$
	0	14.12815	23 944	$g = 2.0022 \pm 0.00017$
Tritium	$I_z' = \frac{1}{2}$	13.67683	23 942	$A = 1515.3 \pm 0.4$
	$-\frac{1}{2}$	14.57270	23 942	$g = 2.0019 \pm 0.00017$
Hydrogen	$I_z' = \frac{1}{2}$	13.70655	23 941.5	$A = 1418.6 \pm 0.4$
	$-\frac{1}{2}$	14.54599	23 943	$g = 2.0021 \pm 0.00017$

[28] P. Kusch, Phys. Rev. **100**, 1188 (1955); R. Beringer and M. A. Heald, *ibid.* **95**, 1474 (1954); A. G. Prodell and P. Kusch, *ibid.* **79**, 1009 (1950); **88**, 184 (1952).

[29] L. W. Anderson, F. M. Pipkin, and J. C. Baird, Jr., Phys. Rev. **120**, 1279 (1960).

[30] F. M. Pipkin and R. H. Lambert, Phys. Rev. **127**, 787 (1962).

[31] A. Abragam, *Principles of Nuclear Magnetism* (Oxford University Press, New York, 1961).

$6\frac{1}{2}$ Å, or twice the lattice spacing a. Atoms which come closer together than this must surely recombine rapidly, which makes 80 G a likely cutoff limit.

Another perhaps more cogent argument discourages a refined application of the Kittel-Abrahams theory. This theory is predicated upon the idea that the lattice sites (or interstices) are occupied randomly by the unpaired atoms. The close-lying atom pairs necessary to produce the large fourth moments demanded by the Kittel-Abrahams theory would, therefore, occur in proportion to the square of the atomic concentration, being produced at a rate proportional to the concentration. Such a growth of broad line sites is inconsistent with the data of Fig. 9, which show that the broadline sites build up uniformly from time $t=0$.

The line breadths of the broad line components therefore reflect *intrinsic* properties of the broad line sites, although they may be affected incidentally by a statistical overbroadening of the Kittel-Abrahams type.

It should be noted in connection with the Kittel-Abrahams theory that the process of formation of the atoms by dissociation *in situ* of D_2 molecules will tend to produce a random arrangement of *pairs* of atoms rather than a dispersal of solitary atoms. According to the Bethe formula[32] for the stopping power of nonrelativistic electrons in solid D_2, the tritium betas should lose about 20- —40-MeV of energy/cm of path length. If 2.2% of this energy goes into dissociation of the D_2 molecules, then atomic pairs will be created at mean intervals of about 1000Å along each beta track. When the molecules are dissociated, the two daughter atoms will fly apart with about $3\frac{1}{2}$ eV of kinetic energy each, the Franck-Condon principle[17] requiring the bombarding particles to transfer much more energy to the D_2 molecule than the recombination energy of 4.4 eV. Although the atomic kinetic energy is rather large compared to the heat of fusion of solid D_2, which is about 0.016 eV/molecule, it will require only 13 or 15 collisions to thermalize the daughter atoms. Because they are scattered by appreciably heavier scattering centers, there will be considerable backward scattering; and when the thermalization process is complete, the two daughter atoms will have an appreciable probability of finding themselves within 10 lattice sites of each other.

These considerations suggest that the broad line sites might be produced by the perhaps 10% of the thermalization processes which result in the atoms being immobilized within two or three lattice spacings of each-other. It also points towards an explanation of the difference between the ESR spectra observed in samples made by freezing tritiated D_2 and those observed[3] in samples made by condensing a deuterium discharge. There should be a smaller tendency for atoms in the latter samples to clump in pairs, and the samples should not give rise to EPR lines so broad as those we have observed.

[32] Enrico Fermi, *Nuclear Physics* (University of Chicago Press, Chicago, 1950).

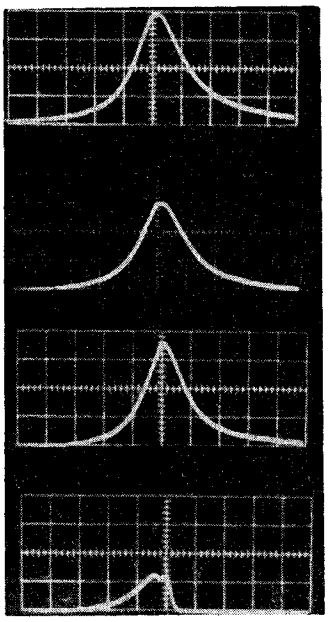

FIG. 14. Transient saturation of the high-field composite D line. Sample age, 5 days. Microwave power levels are, from top to bottom: 0.5, 5.5, 55, and 600 μW. The time scale is 0.010 sec per major division, with time increasing towards the right. The extra bump in the bottom trace is evidence of the composite nature of the line.

As in the case of the resonances in young samples, the broadline components are homogeneously broadened, as shown by the oscillographs of Fig. 14. These oscillographs reveal an astonishing fact. As the microwave power level is increased, the ESR lines diminish in intensity as expected, but then *narrow* and *increase* in strength before, finally, sinking back as the power level is further raised. This feature was exhibited under quasistatic conditions as well. Recorder tracings of the derivatives of the lines demonstrated that, while the broad line component diminished in intensity as expected, the narrow line component showed an *enhancement* of nearly 2 as the power level was raised through the appropriate region. It is likely that this anomalous behavior of the narrow line component is responsible for the undue shortness of the narrow line spin-lattice relaxation time estimated from (41) and (33). It may also explain the unexpected sharpness of the knee of the saturation data of Fig. 15.

Relaxation

Relaxation measurements taken on old samples by the double passage technique already described yield, as do the younger samples, semilog plots which can be fitted by straight lines within experimental error. The relaxation is, therefore, again characterized approximately by a single exponential whose time constant is 0.220 ± 0.035 sec. That the matter cannot be allowed to rest so simply, however, is demonstrated by the tracings of Fig. 16, which show consecutive passages through all three D lines followed by a reverse passage. These tracings were taken under approximately the same power levels as those under which the "approximately exponential" relaxation was measured. It is evident that the three D-resonance lines in old samples are not inde-

pendent under saturation conditions, for saturation of the first line of the triplet lowers the intensity of the second line, and so on. The effect does not depend on the sense in which the lines are traversed.

Although excitation of the very weak transitions P (Fig. 6) between successive traversals of the allowed transitions could produce an intensity degradation pattern qualitatively similar to that observed, the degradation set in at power levels as little as 10 dB above that required to elicit saturation of the individual resonances, and some mechanism more powerful than microwave-induced P transitions must be involved. We believe that mechanism to be a fluctuation of the local magnetic field at the broad line sites which has a high spectral density at frequencies near 109 Mc/sec, which is the spacing of the hyperfine sublevels of the Zeeman multiplets. Such fluctuations could induce as relaxation processes the diagonal transitions Q of Fig. 6. If relaxation by R and P transitions could be neglected during traversal of the three lines, and if Q transitions were capable of bringing the multiplet sublevels into equilibrium in the time between successive lines, one would find at high power levels an intensity pattern of 9:6:4. Part of the failure of the lines to achieve this pattern is no doubt due to the effectiveness of relaxation by R processes in competing with the Q processes; application of the theory developed earlier for the case $Q \gg R$, P leads to the value $(2Q)^{-1}=0.130\pm0.020$ sec, which is not much shorter than the value $(2R)^{-1}=0.220\pm0.035$ sec estimated from semilog plots of the fractional recovery of the electronic polarization.

Unavoidable variations in the rate at which the external field is swept through the resonances are a formidable source of distortion of the pattern, since they lead to unpredictable changes in the point on the shoulder of a line at which saturation overwhelms the relaxation mechanisms. Significant changes in the pattern were in fact observed when the sweep over the three lines was

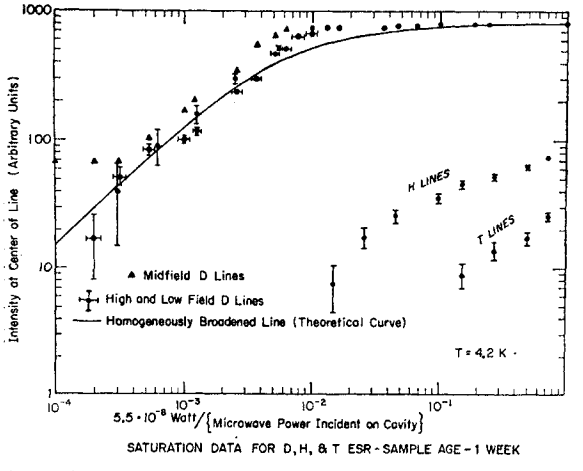

FIG. 15. Saturation data from a well-aged sample. The carrier level at the mixer crystal was kept constant, as described in text.

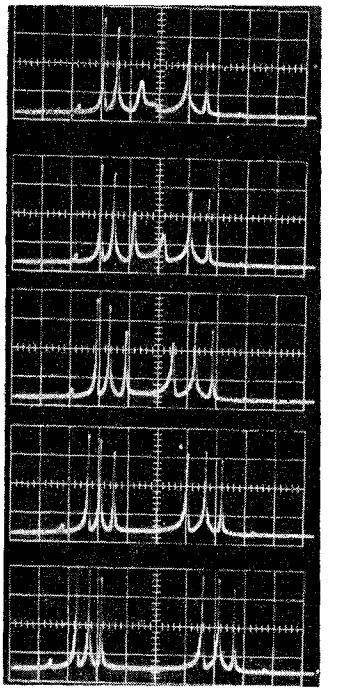

FIG. 16. Interline relaxation. The magnetic field is swept back and forth by a triangular voltage waveform. Time scale in all traces is 0.200 sec per major division, with time increasing towards the right. Sample age, 19 days. $T=4.2$°K.

obtained from the "linear" portion of a sinusoidal driving voltage instead of from the rising portion of the triangular waveform normally used. For this reason, no analysis of these patterns will give completely reliable values of Q and R. The values just listed are felt to be reasonably accurate, however.

It is interesting that these values of Q and R are roughly compatible with the simplest model[15] which can be formulated for the field fluctuations at the broad line sites; to wit, that the correlation function is a simple exponential with characteristic or correlation time τ_c which is long compared to all the inverse frequency spacings of the levels of Fig. 6. The Fourier spectrum $g(\omega)$ of the exponential correlation function is proportional to $(1+\omega^2\tau_c^2)^{-1}$, and if $(2\pi\tau_c)^{-1}$ is comparable to 109 Mc/sec the ratio of the spectral density at this frequency to that at 24 000 Mc/sec will be about 48 000:1. Now any operator that induces an R transition is also capable of inducing Q transitions, though with a matrix element some 150 times weaker. If the squares of the matrix elements are weighted with the respective spectral densities, however, the transition rates will be comparable.

Temperature-Dependent Effects

The D-atom relaxation times observed in the well-aged samples were disappointingly insensitive to changes in the temperature of the lattice, the line patterns obtained at 1.2°K differing insignificantly from those observed at 4.2°. Rather astonishing changes occurred in the line breadths, however, the breadths appearing to vary inversely with temperature over this tempera-

ture range. The full width at half intensity was 44.5±0.5 G at 1.17°K. The peak amplitudes of the D resonances remained at the values they had had at 4.2°, even over storage times up to ten hours in length at 1.2°. The changes in the areas of the resonance curves may thus be ascribed entirely to the lowering of the sample temperature; there is no increase, upon lowering the temperature, of the saturation concentration of unpaired atoms.

The broadening of the lines without any apparent increase in the number of atomic centers suggests that lines arising from broad line sites (the breadth of the narrow line sites, observed in young samples, was independent of temperature between 1.2° and 4.2°) are motionally narrowed[15] at 4.2° and achieve their full widths only at temperatures of 1.2° or below, where the narrowing motions are adequately frozen out. The lines will not be narrowed from their static half-widths unless the inverse of the correlation time of the local field, or other broadening mechanism, is of the order of the half-width, expressed in rad/sec, or larger. Only the components of the local field's spectral density which lie between zero frequency and the frequency equal to the half-width of the observed line should be effective in broadening the resonance line, for the effects of higher frequency components must average to zero.[15] If a Lorentzian spectral density is assumed, it is found that a correlation time of (190 Mc/sec)$^{-1}$ will produce a narrowing of the half-width from 22 G to the observed 5.4 G at 4.2°. Using this value, the spectral density at 109 Mc/sec becomes about 20 000 times that at 24 000 Mc/sec. One therefore expects, if the broadening interaction is also responsible for the broad line site relaxation, that $Q=\frac{5}{6}R$. It is striking, but perhaps fortuitous, that this prediction corresponds so closely to the results obtained from the relaxation studies.

One apparently irreversible change occurred in the D-line shapes upon refrigeration to 1.2° and subsequent warming to 4.2°. One component of the composite lines shifted somewhat with respect to the other, so that the narrow line peak could be noticed as a tiny bump on the low-field side of the highest point of the over-all line profile. The displacement appeared to be about 2 G and was the same for all three lines.

Lowering the temperature did not produce the same effects on the T and H lines as on the D lines. The peak intensities increased somewhat, and the half-widths increased by a factor of only 2 over the range from 4.2 to 1.2°.

CONCLUSIONS

Spin-Lattice Relaxation Times

It is apparent from Fig. 15 that the T and H resonances saturated at power levels as much as 20 dB below those at which the D resonances were affected. The relaxation times of these weak resonances were estimated by observing the asymmetry produced in their derivatives during slow, moderately saturating back-and-forth passages of the magnetic field and were found to be about 2 sec or longer. The same was true of the D lines in samples less than 5- or 10-min old. But why do the T and H lines retain their long relaxation times as the sample ages while the D lines do not?

A rather satisfying answer occurs in Bloembergen's concept[33] of spin diffusion, in which angular momentum is transferred from spin to spin by mutual flip-flop processes. Spins having equal resonant frequencies can participate in flip-flops without interchanging energy with the lattice, and the diffusion will proceed rapidly; for, unlike spins, the flip-flops do not conserve magnetic energy and cannot proceed without direct participation by the lattice, which inhibits the diffusion.

The model we shall employ here supposes that the broad line sites and the narrow line sites have intrinsic relaxation times, at vanishing concentration of unpaired atoms, of 0.220 and 2 sec, respectively. The relaxation time of the narrow line resonance observed in our practical samples is affected, through spin diffusion, by the presence of the broad line sites. The electronic angular momentum of a narrow line D atom in, say, the $I_z'=1$ state may be transferred to a broad line $I_z'=1$ atom which absorbs the angular momentum and then undergoes a spin-lattice relaxation process. The broad line D spin has therefore relaxed, in effect, a narrow line spin. Because the concentrations of T and H atoms are so much lower than that of D atoms, their spin diffusion is less rapid; because there are few (if any) broad line T and H centers, the spin diffusion will not materially shorten the T or H relaxation.

Quantitative predictions of the model are in good agreement with the experimental results. According to the argument developed by de Gennes[34] if the relaxation time of the broad line component were very short, the observed relaxation time, τ_1, of the narrow line component would be on the order of

$$\tau_1^{-1}=4\pi NbD\approx 8\pi f(H_0)\mu_0^3/d^6\hbar\,, \qquad (42)$$

where N is the number of broad line centers per unit volume, D is the Bloembergen diffusion constant, b is the so-called "scattering length," and d is the mean distance between nearest-neighbor atoms of the same hyperfine species. Assuming a concentration of 33 atoms per million lattice sites, one finds $\tau_1=4\times10^{-3}$ sec, which means physically that the diffusion of narrow line polarization occurs much more rapidly than the rate with which the broadline centers can relax it. The model predicts for T and H atoms a τ_1 of about 2500 sec, which means that only the intrinsic relaxation of these lines would be observed. The model appears, when applied less crudely than in Eq. (42) to explain also the inverse dependence of the D relaxation time upon the concentration during the initial growth region of Fig. 9.

[33] N. Bloembergen, Physica **15**, 386 (1949), exp. p. 410 ff.
[34] P.-G. de Gennes, J. Phys. Chem. Solids **7**, 345 (1958).

A Comparison to Results in T_2 and in HD

It is puzzling that the D-atom spectra were composite while the T and H spectra seemed to be devoid of unusual structure. Lest we be led into attributing the broad line D sites to the fact that deuterons have a spin of 1 as against spin $\frac{1}{2}$ for T and H, we performed some experiments on pure solid T_2 and on a sample consisting of 400 cm³ (NTP) of HD and 4-cm³ T_2. In one of the solid T_2 samples the lines gave true evidence of composite structure, but in the remaining samples of T_2 this structure seemed absent, suggesting that the rate of condensation of the pure tritium could strongly influence the rate at which broad line centers built up. Because of the comparatively high concentration of decaying nuclei in the pure tritium samples, we feel it unwise to exact a comparison of the behavior of these samples to that of the D_2 samples.

In the HD samples the evidence pointed unambiguously toward the existence of two lattice sites for the H atoms. Samples less than 1-h old gave simple absorption derivatives. As time went on, the center of the derivative tracing began to flatten out and the wing opposite the nearby tritium line to broaden, all without changing the amplitude of the derivatives seen at one hour. At a sample age of two days the high-field H line had taken on the appearance presented in Fig. 17, whose features may be qualitatively reproduced by superposing two nearly identical absorption derivatives so that the positive peak of one falls over the negative peak of the other. The low-field H line appeared to be a mirror reflection of the high-field line, which shows that the centers responsible for the two lines differ more in hyperfine splitting than in g value. The hyperfine structure interactions of the two sites differ by about 0.8%.

The H lines may be regarded as continuing the behavior of the D lines described earlier, the relative displacement of the two components magnified in proportion to the hyperfine interaction constant of the free atom. That in this case the two components have about the same breadth arises from the fact that the nuclear moments in the HD molecule can produce, at a given distance, about twice the magnetic field of a D_2 molecule, which makes the appellation, "narrow line site," rather inappropriate at 4.2°.

That the broad line site is truly broad line was revealed when the sample temperature was lowered to 1.2°; the widths of the composite lines reached 25 G. Apparently, lower temperatures would have been required to recover the full breadth of the lines. The similarity of the H lines to the composite D lines observed earlier was demonstrated in the line narrowing under transient saturation at 1.2°. The line derivatives at 4.2° reverted to the simple form as the steady saturation region was entered.

The relaxation times of the lines in the HD samples were of the same order of magnitude as those in the D_2 samples. The composite H lines in HD appeared in-

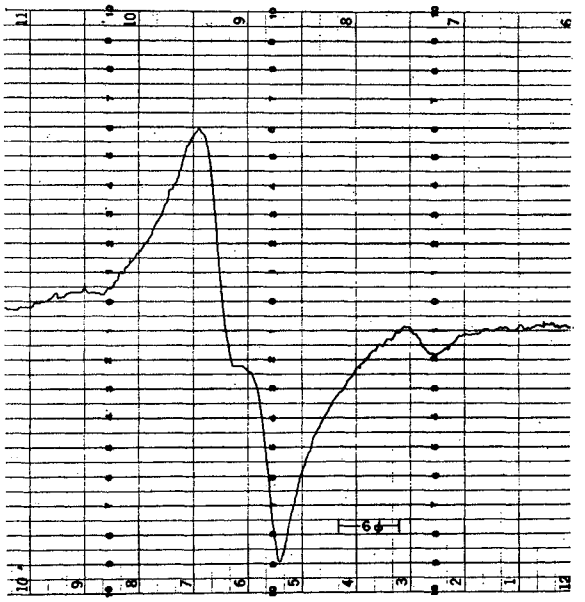

FIG. 17. The derivative of the absorption components of the high-field T and H lines in HD. The T line is the small structure at the right. The low-field line is a mirror reflection. Sample age, 2 days.

homogeneously broadened at 4.2°, which suggested that the spin diffusion has been hindered by the resolution of the two resonance frequencies. A pair of barely resolved, homogeneously broadened lines might, therefore, take the appearance of a single inhomogeneously broadened one in our transient saturation studies.

The reason why the H and T lines from the D_2 samples remained simple is probably to be found in the relative rates of buildup of the two types of sites. Were broad line T and H sites to become populated at only 9% of the rate for narrow line sites, it would have required about 2 months of storage at 4.2° before the T and H lines took on an appearance analogous to that of the D lines. The behavior of the T and H lines in the D_2 samples suggests that broad line T and H sites were being formed rapidly while the sample was cooled below 4.2°. It seems then that the lower temperatures would promote the formation of the broad line sites.

Linewidth

The direct experimental evidence obtained from the transient saturation studies has shown that the D ESR lines may be regarded as homogeneously broadened, at least over the intervals as long as the several milliseconds required for the magnetic field to pass through the line. We here assert that the lines must be homogeneously broadened in the classical sense, having values of spin-spin-relaxation time,[15] T_2, actually equal to the inverse of the half-width expressed in cycles/sec. We have already made an assumption tantamount to this assertion in our calculation [Eqs. (33) and (41)] of T_1 for the narrow line sites, in which we used the observed un-

saturated line shape to compute the transition probability per atom, W. Were the line inhomogeneously broadened, consisting of a superposition of spin packets of breadth very small compared to that of the over-all line, the appropriate theoretical treatment[27] would have led to a calculated value of T_1 perhaps orders of magnitude shorter than that observed.

The factor of two by which the relaxation time calculated from the saturation data exceeds the measured relaxation time seems due to the same mechanism which produced the line narrowing and intensification of the composite line observable in Fig. 14. We demonstrated that the narrowing and intensification occurred independently of large concentrations of broad line sites by examining the narrow line resonance in a young D_2 sample which contained only about 1% of the tritium concentration that we had heretofore used. As the intensity of the microwave power incident upon the cavity was increased in the usual way, the three resonances observed in transient passage appeared to narrow somewhat and, up to a power level of 55 μW, to diminish somewhat in amplitude. Suddenly, as the power level was increased to 190 μW, the resonance amplitudes increased to about 1.5 times their unsaturated values. At 620 μW the amplitude had descended to about $\frac{2}{3}$ the unsaturated value, and it decreased in normal fashion thereafter. Small concentrations of broadline centers had been present during these measurements, as we noted from the double-humped character of the highly saturated line. The three lines remained equal in amplitude well into the saturation region.

Computations based upon Fig. 15 and Eq. (33) lead to underestimations by a factor of 2 to 5 of the observed relaxation time of the broad line component; but such calculations cannot be regarded as definitive, in view of the composite nature of the line. We have no evidence to believe that the broad line component behaves differently from typical homogeneously broadened lines.

The narrow line component seems to have homogeneous character, but cannot be characterized by a value of T_2 which is independent of the applied rf field.

ACKNOWLEDGMENT

We should like to thank Jack T. Sanderson for his very considerable contributions to the construction of the microwave spectrometer and to the gas discharge experiments which served as preliminaries for those described here.

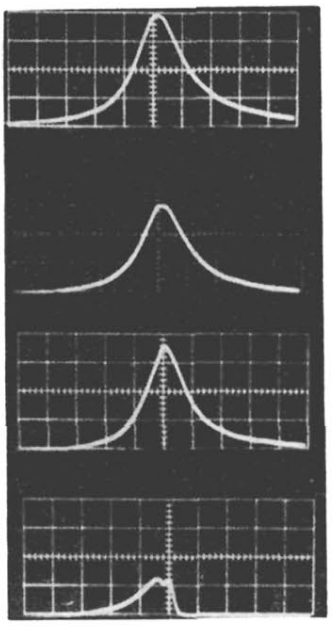

FIG. 14. Transient saturation of the high-field composite D line. Sample age, 5 days. Microwave power levels are, from top to bottom: 0.5, 5.5, 55, and 600 μW. The time scale is 0.010 sec per major division, with time increasing towards the right. The extra bump in the bottom trace is evidence of the composite nature of the line.

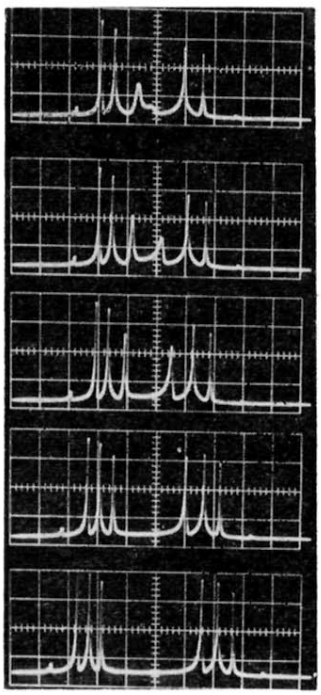

FIG. 16. Interline relaxation. The magnetic field is swept back and forth by a triangular voltage waveform. Time scale in all traces is 0.200 sec per major division, with time increasing towards the right. Sample age, 19 days. $T=4.2°K$.

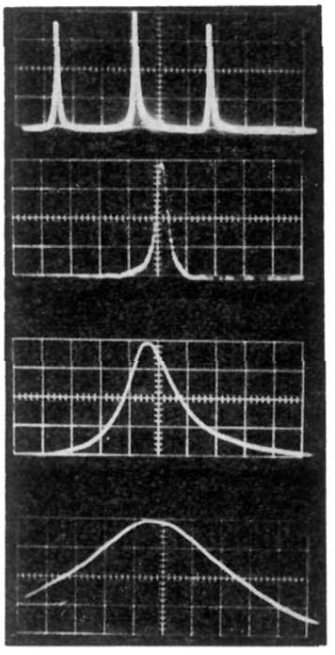

FIG. 8. Typical oscilloscope displays. Above: The 3 D lines at 4.2°K and sample age 23 min. Peak spacing is 78 G. Below: high-field D line at fivefold sweep magnification. Sample ages 12 min, 6 days, and 6 days. In bottom oscillograph $T = 1.2°$.